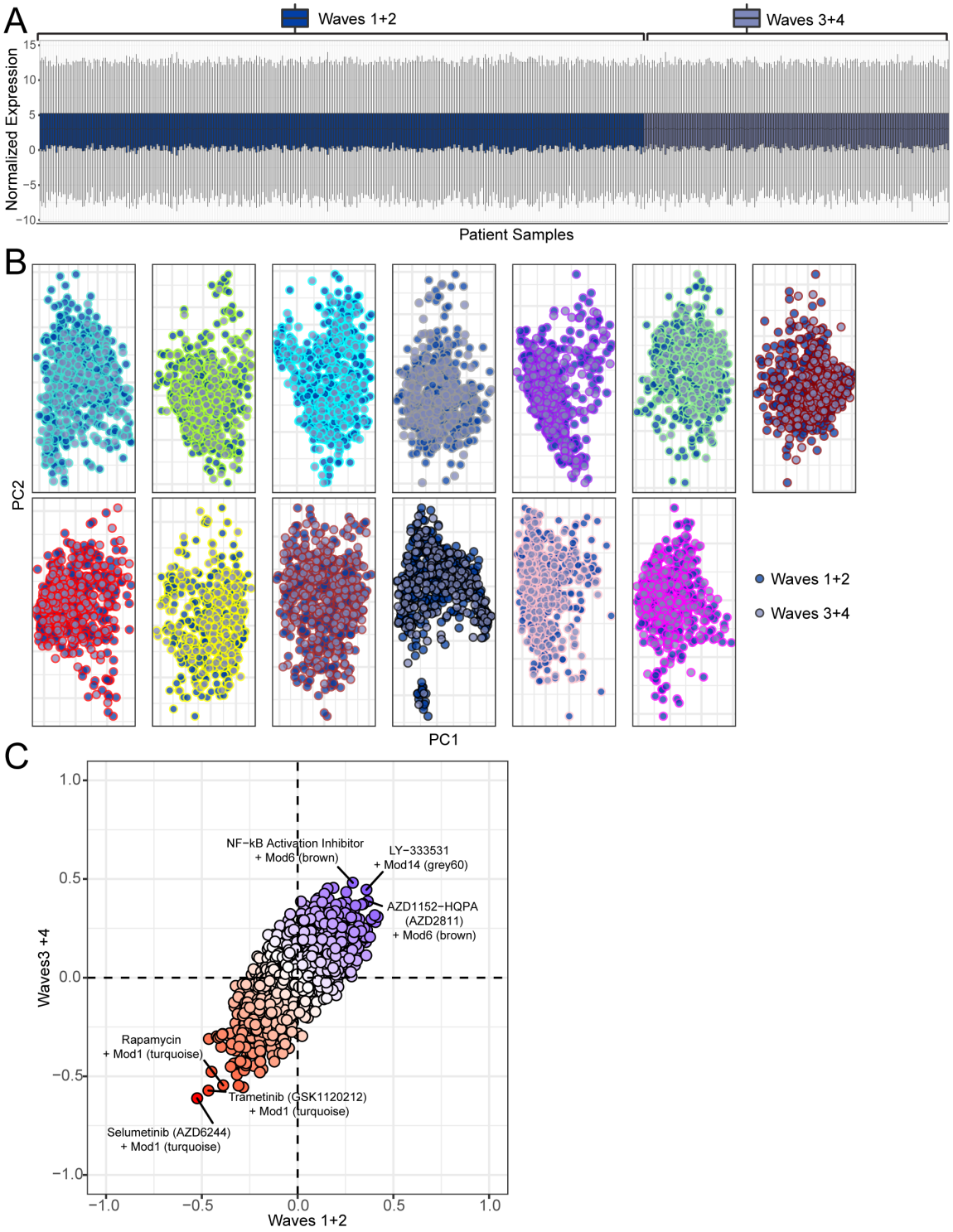

Figure S1. Normalized Expression by Cohort, Related to Figure 1. (A) To harmonize the RNAseq gene expression data across Waves, we used the reference distribution and parameters learned from the conditional quantile normalization (CQN) performed on the Waves 1+2 cohort and applied these to Waves 3+4 samples. The resulting values were comparable as judged by boxplots of the distribution of normalized gene expression (Y-axis) vs patient sample (X-axis). The boxplots are colored as presented in Figure 1A. (B) We examined consistency of WGCNA gene expression profiles by plotting each Waves 1+2 and Waves 3+4 samples for each WGCNA module after principal component analysis. The first two principal components of WGCNA expression profiles generated in Waves 3+4 are highly overlapping with respect to range and clustering relative to Waves 1+2, suggesting feasibility of re-use of WGCNA modules. (C) We evaluated agreement of the correlation between ex vivo drug response and WGCNA module eigengene values between Waves 1+2 and 3+4. For both cohorts we computed the Pearson's correlation between each WGCNA module eigengene and the AUC of each inhibitor. At least 30 patient samples were required for each module/inhibitor combination. The points are colored by the average correlation between waves with respect to the sensitive (red) to resistance (blue) scale defined in Figure 3A. The top 3 sensitive and resistant relationships are called out in text.

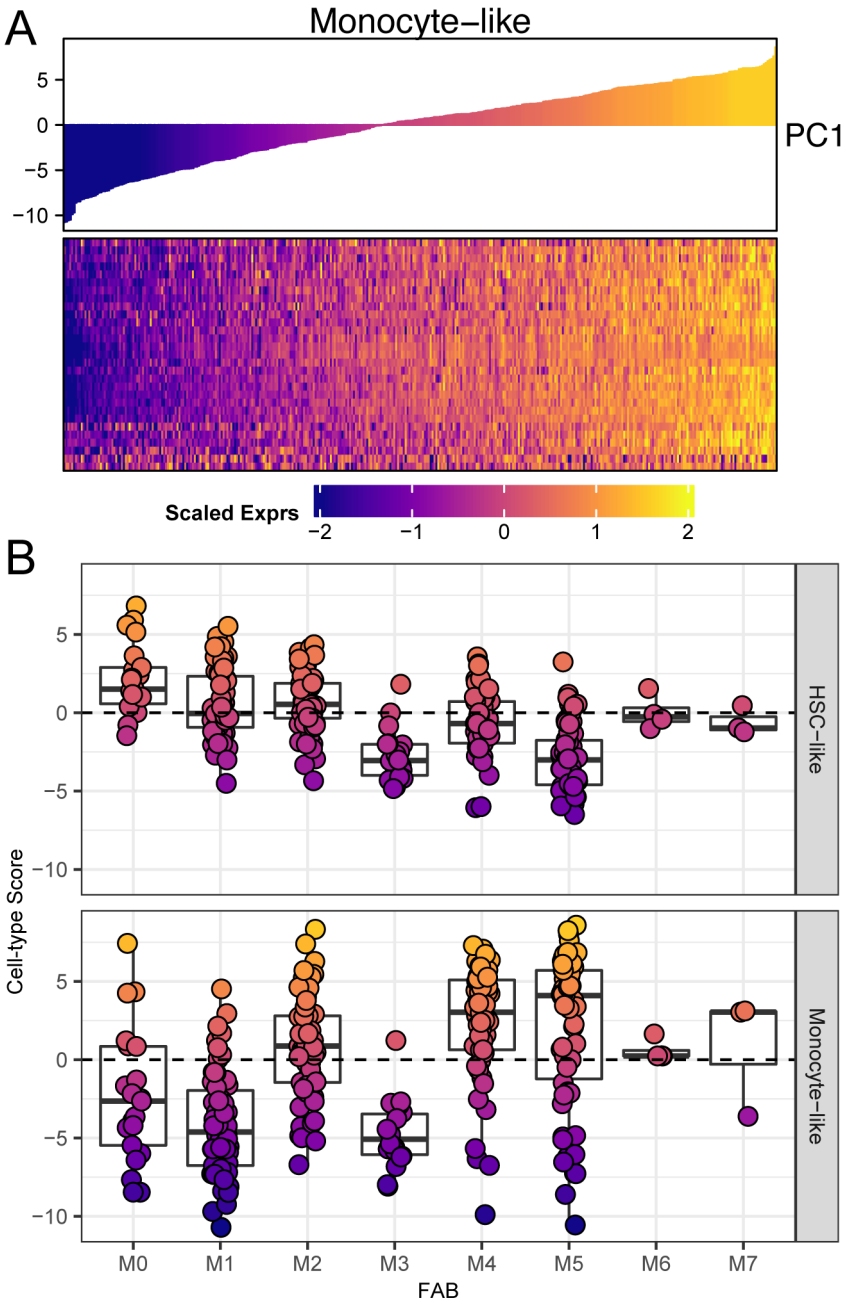

Figure S2. Differentiation scoring correlates with clinical annotation of tumor maturation state, Related to Figure 2. We generated malignant cell-type scores for each of our patients relative to 6 sets of 30 genes derived from expression signatures from single-cell sequencing (Van Galen et al., 2019). (A) Similar to the eigengene methodology of WGCNA (shown in Figure S1), cell-type scores were computed as the first principal components (top barplot) of each cell-type gene set (heatmap) where rows are genes and columns are the samples from Waves 1+2. We then computed the scores for Waves 3+4. (B) Comparing the combined set of scores with FAB blast morphology classification, we see that the HSC-like and Monocyte-like scores are inversely related across the FAB classifications (M3 being an exception). As expected, the highest scores in the HSC-like category are in the lower FAB categories (M0-2) whereas the highest Monocyte-like scores are in the more differentiated M4-5 categories.

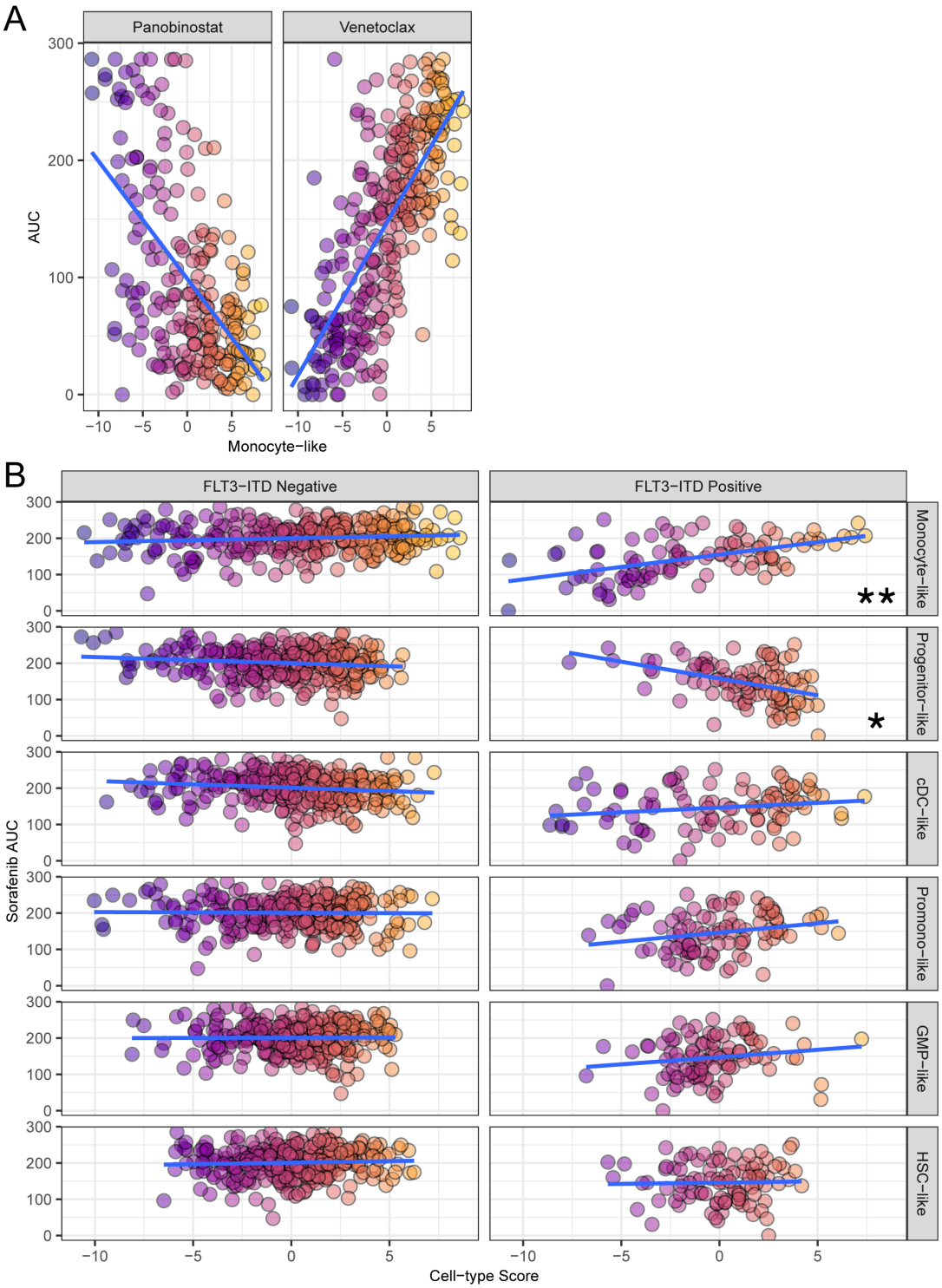

Figure S3. Cell-type inhibitor correlations, Related to Figure 3. (A) The two outlier inhibitors from Figure 3A, Panobinostat and Venetoclax, are shown to have an opposing linear relationship with the Monocyte-like score. The color scheme follows the high (yellow) vs low (purple) gradient for cell-type scoring. (B) Sorafenib sensitivity that correlates with FLT3-ITD status in a manner that is conditional on cell-type score as in Figure 3B is shown. Sorafenib shows no discernible association with cell-type scores in the FLT3-ITD negative subgroup. However, in the FLT3-ITD positive subgroup opposing linear associations with Monocyte-like and Progenitor-like scores can be seen (statistical analysis provided in Figure 3B).

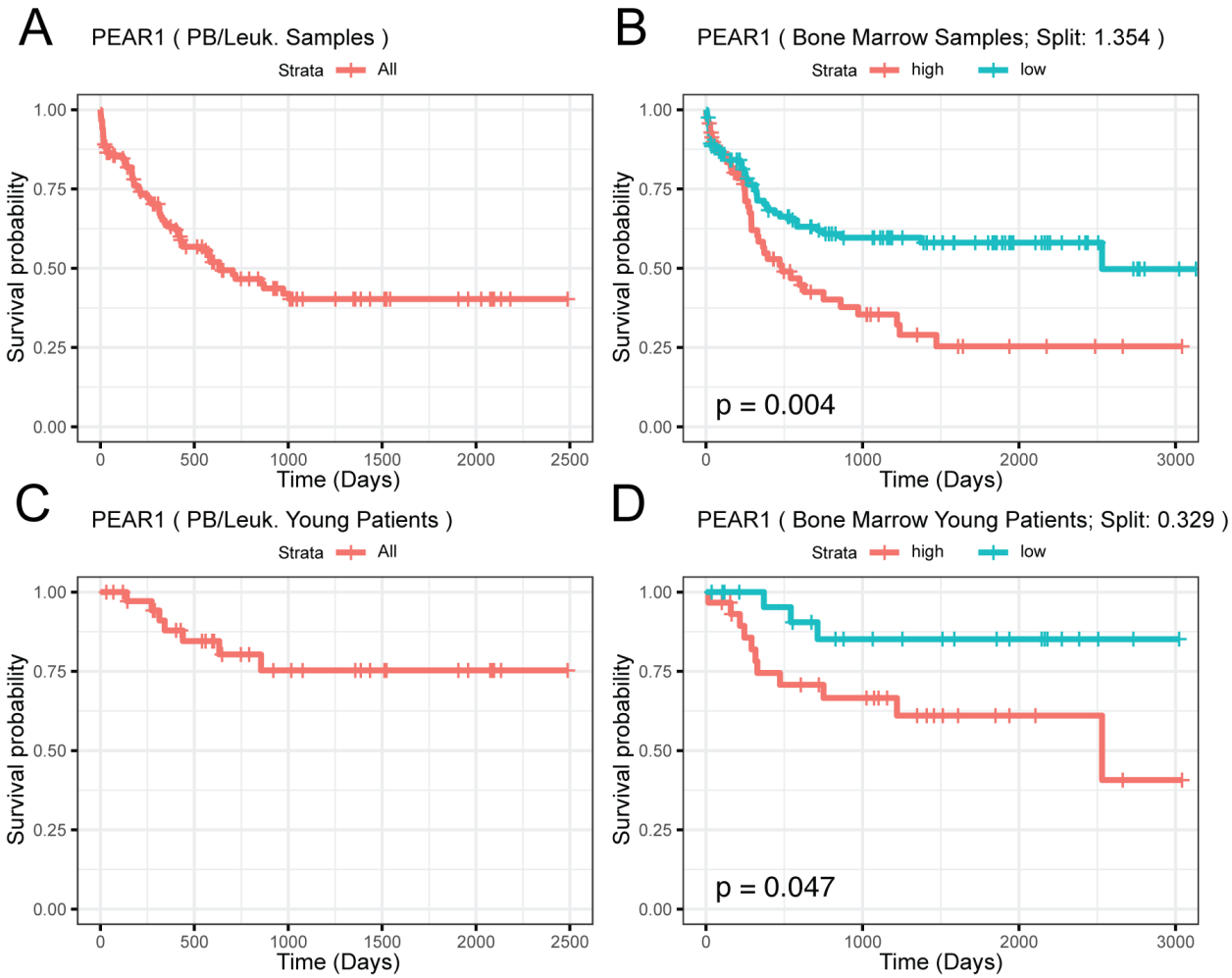

Figure S4. Prognostic association of PEAR1 is dependent on originating tissue type, Related to Figure 6. Considering the entire cohort of Denovo patient RNASeq samples with survival information and limiting to peripheral blood or leukapheresis samples, we cannot find a significant split of PEAR1 using a conditional inference tree (ctree) (A). However, using bone-marrow derived samples allows us to differentiate prognostic groups (B). Focusing on the young cohort (<45 years), prognostic groups are again only able to be formed using a ctree approach in the bone-marrow derived samples (C-D); Significance was determined using the Log Rank test.

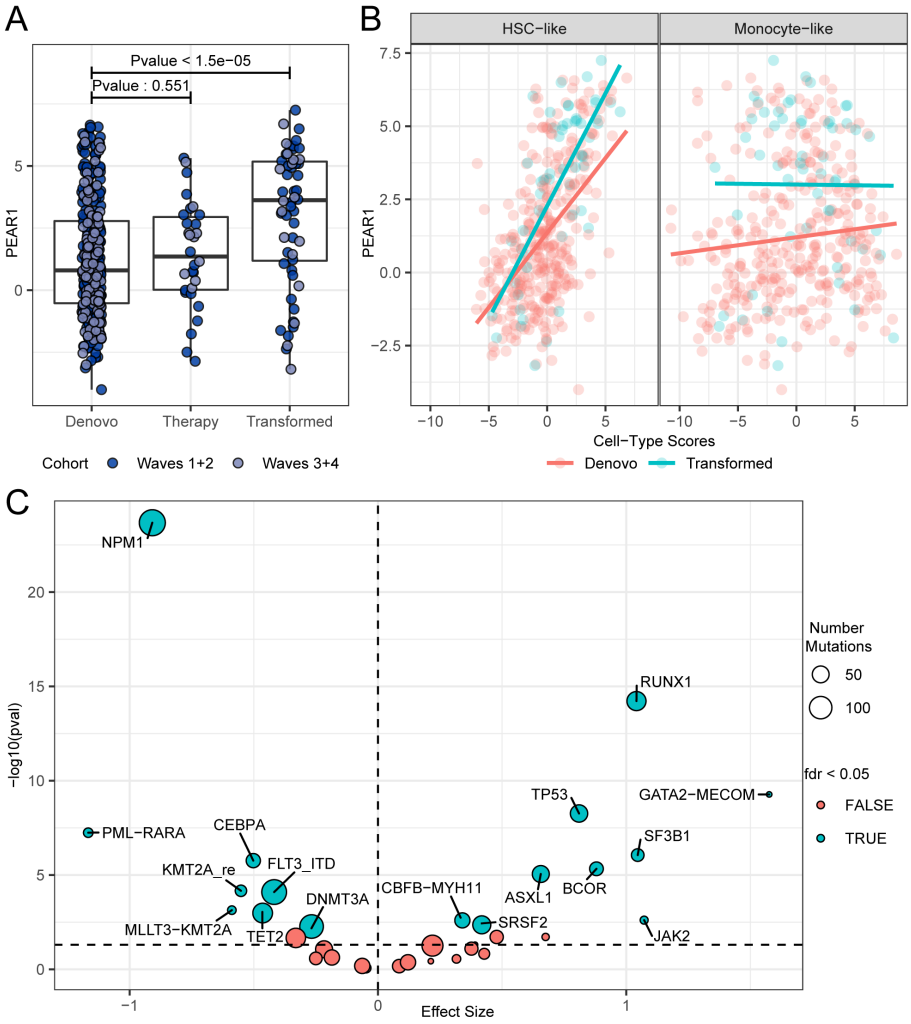

Figure S5. Mutational and clinical association with PEAR1 expression, Related to Figure 6. (A) Patients that had a prior MPN, MDS, or MDS/MPN diagnosis (Transformed) were seen to have significantly higher PEAR1 expression (Welch's T-test Pvalue < 1.5e-05) than those that had AML diagnoses without a known originating factor (Denovo). Expression values for both cohorts were evenly represented in the diagnosis groups. (B) This significant increase in PEAR1 expression for Transformed patients relative to Denovo was seen across the range of the Monocyte-like cell-type scores, however, a significant interaction was observed with respect to the HSC-like score (Pvalue=0.024). (C) For each AML mutation and fusion, we computed the difference in average PEAR1 expression between mutated and wild type (shown as points with size given by the number of mutated samples). This difference is reported in terms of a standardized effect size (Glass's delta relative to wild type; x-axis). The vertical dashed line indicates mutational association with increased expression on the right, and with decreased expression on the left. Unadjusted significance of these differences is given on the y-axis with a dashed line indicating the 0.05 level. Blue genes indicate those that are significant (BY FDR < 0.05; (Benjamini and Yekutieli, 2001)), red otherwise.

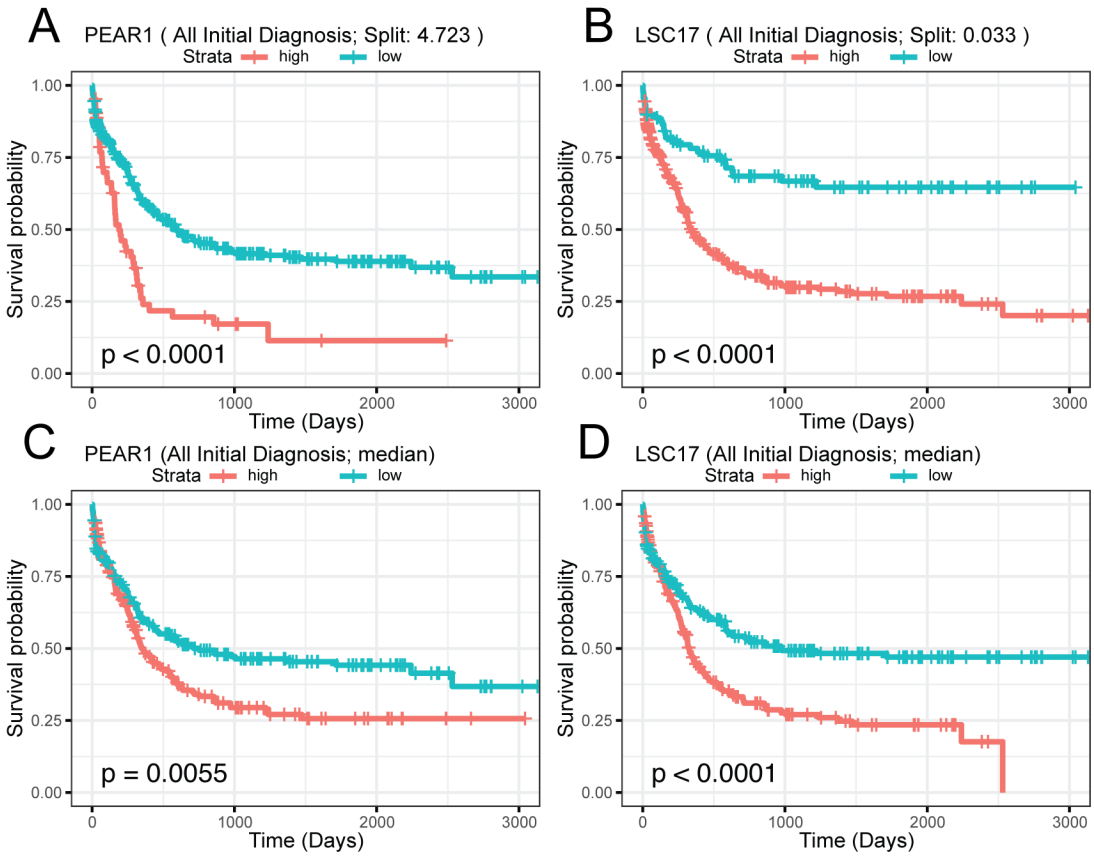

Figure S6. PEAR1 has prognostic ability in entire cohort, Related to Figure 7. PEAR1 performs similarly to the LSC17 signature when using all waves 1-4 cohort specimens that were obtained at initial acute leukemia diagnosis with splitting defined using our conditional inference tree methodology for both (A-B) or split based on the median values for both (C-D) (as described in (Ng et al., 2016) for LSC17).

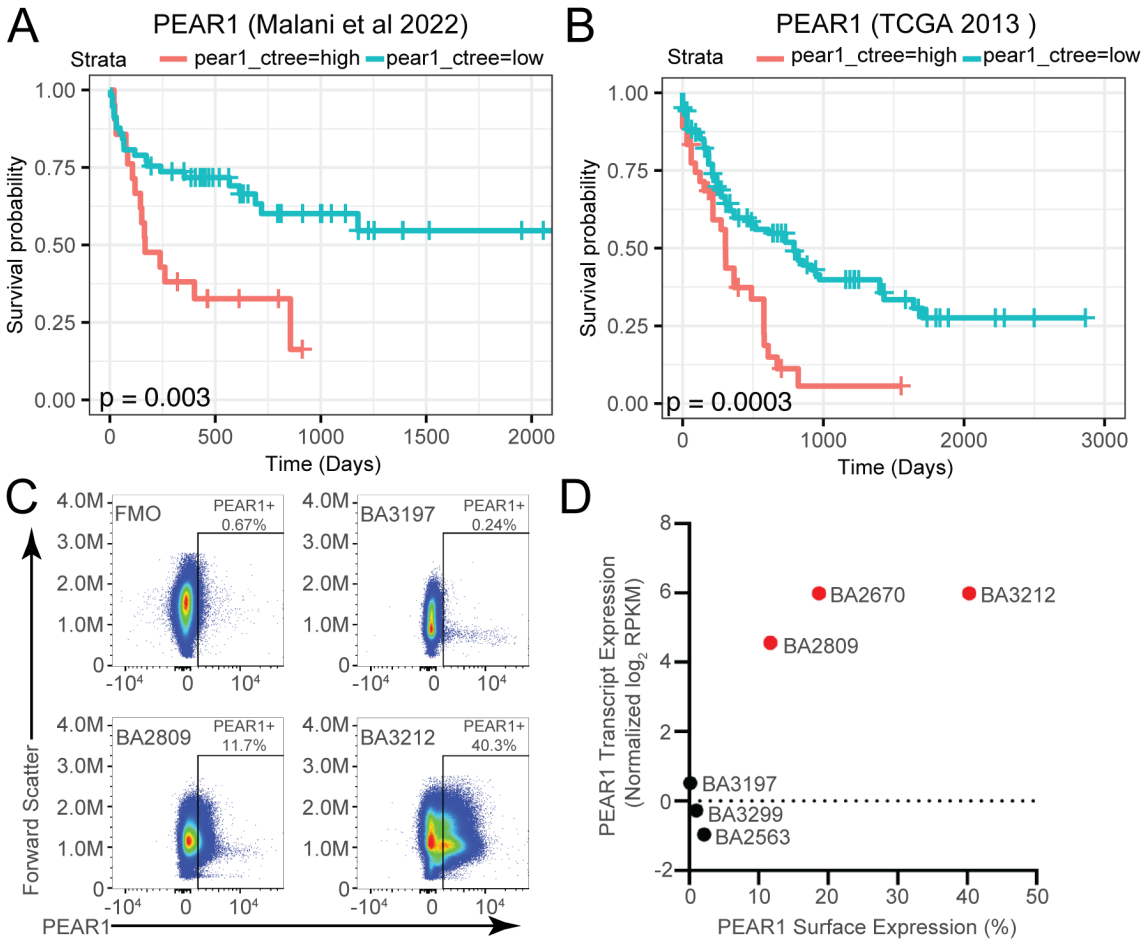

Figure S7. PEAR1 expression validates as a prognostic factor in two independent AML cohorts and validates as a potential therapeutic target by flow cytometry, Related to Figure 7. (A) Significant survival differences based on PEAR1 gene expression were seen in the (Malani et al., 2022) cohort (P-value: 0.003; n=78), all of which were bone marrow derived initial diagnosis samples. In addition, significant survival differences were also seen after adding in the peripheral blood samples (P-value: 0.0004; n=84, figure not shown). As several library preparations were carried out, we additionally assessed the effect of limiting samples to only the Illumina ScriptSeq v2™ library preparation. We again saw significant survival differences in the bone-marrow derived samples (P-value: 0.02; n=69, figure not shown) and the combined peripheral blood and bone marrow samples (P-value: 0.001; n=74, figure not shown). (B) Significant survival differences were also seen based on PEAR1 expression in the (Cancer Genome Atlas Research et al., 2013) AML cohort (P-value: 0.0003, n=150). PEAR1 groups were determined based on our conditional inference tree methodology as described in the methods. Significance was assessed between the two groups using the log rank method. (C) Cells from 6 AML patient specimens were stained with fluorescently conjugated anti-PEAR1 antibody and analyzed by flow cytometry. Live, single cells were gated for PEAR1 positivity by comparing to a fluorescence minus one (FMO) control. The plots for forward scatter versus PEAR1 are shown for the FMO and three of the six samples. (D) PEAR1 positive surface expression, as measured by flow cytometry in (C) was compared with normalized PEAR1 transcript expression from RNA-seq.